Biosensors and Bioelectronics 214 (2022) 114529

Contents lists available at ScienceDirect

Biosensors and Bioelectronics

journal homepage: www.elsevier.com/locate/bios

Fluorescence imaging of FEN1 activity in living cells based on controlled-release of fluorescence probe from mesoporous silica nanoparticles

Yanhua Tang [a,1], Duoduo Zhang [a,1], Ye Lu [a], Songqin Liu [a], Juan Zhang [b], Yuepu Pu [b], Wei Wei [a,*]

[a] Jiangsu Engineering Laboratory of Smart Carbon-Rich Materials and Device, School of Chemistry and Chemical Engineering, Southeast University, Nanjing, 211189, China

[b] Key Laboratory of Environmental Medicine Engineering of Ministry of Education, School of Public Health, Southeast University, Nanjing, 210009, PR China

ARTICLE INFO

Keywords:
Flap endonuclease 1
Mesoporous silicon nanoparticles
Molecular gate
Controlled-release
Intracellular imaging

ABSTRACT

Flap endonuclease 1 (FEN1) is a structure-specific nuclease, which catalyzes the removal of 5′ overhanging DNA flap from a specific DNA structure. FEN1 has been considered as an important biomarker for cancer diagnosis since it is over-expressed in various types of human tumor cells and closely related to cancer development. Nanoprobes gradually become basic tools for analyzing biomarkers variations in vivo. Here, we utilized aminoated mesoporous silica nanoparticles (NH_2-MSNs) with a rich porous structure as the fluorescence nanoprobes to entrap the rhodamine 6G (Rh6G) molecules. Then gold nanoparticles linked specific single-stranded DNA (AuNPs-ssDNA) as a molecular gate was used to coat the NH_2-MSNs surface. The fluorescence signal was weak when the fluorescence molecules were blocked by the AuNPs-ssDNA. In the presence of FEN1, it recognized and cleaved the specific ssDNA to release the Rh6G from NH_2-MSNs, which resulted in recovered fluorescence signals. Thus, the sensitive detection of FEN1 activity was realized by controlled-release of Rh6G. The fluorescence signal showed a good linear relationship with the logarithm of FEN1 activity ranging from 0.05 to 1.75 U with a detection limit of 0.03 U. Moreover, confocal imaging demonstrated that the proposed biosensor could distinguish tumor cells from normal cells. Therefore, this technique contributes to clinical diagnostic and therapeutic monitoring.

1. Introduction

Flap endonuclease 1 (FEN1) is a flap-specific, multifunctional nuclease and plays an important role in the DNA metabolism pathway (Balakrishnan and Bambara, 2013; Kao et al., 2002). FEN1 is a structure-specific nuclease that cleaves the 5′ single-stranded protrusion (also known as 5′ flap) during Okazaki fragment processing (Pike et al., 2010). FEN1 exists in the cells and has a dynamic localization. It mainly exists in cytoplasm, mitochondria, nuclear stroma, and nucleoli of mammalian cells (Guo et al., 2008; Thompson et al., 2018). Meanwhile, a series of experimental research and evidence show that the FEN1 content in tumor cells is much higher than that in normal cells (Guo et al., 2020; Lu et al., 2020). Over expression of FEN1 is related to multiple forms of tumor progression and therapeutic prognosis, such as hepatocellular carcinoma (Zhang et al., 2020b), testis, breast (He et al., 2016), prostate (Lam et al., 2006), lung (Nikolova et al., 2009), and brain tumors (Zheng et al., 2011). Consequently, FEN1 is a potential broad-spectrum cancer biomarker and an important structure-specific nuclease. It is particularly important to establish a simple, sensitive, and specific method for quantitative detection of FEN1.

During the past few decades, there are various methods for analyzing FEN1. Traditional methods for FEN1 detection are diverse, such as immunohistochemistry, Western blot, and reverse transcription-polymerase chain reaction (RT-PCR) (Ma et al., 2019; Zhang et al., 2018b). But most of them are expenditure of time and effort, and relatively complicated. Therefore, developing sensitive and simple methods for quantitative determination of FEN1 activity is highly essential. Currently, biosensors have been constructed for detecting FEN1, which mainly adopts the method of cyclic amplification to detect the target signal (Li et al., 2021; Zhang et al., 2018a; Zhou et al., 2021). Li et al.

* Corresponding author.
E-mail address: weiw@seu.edu.cn (W. Wei).
[1] These authors contribute equally to this article.

https://doi.org/10.1016/j.bios.2022.114529
Received 2 April 2022; Received in revised form 10 June 2022; Accepted 29 June 2022
Available online 2 July 2022

developed a signal-amplified method based on the cleavage-induced ligation of a dumbbell DNA probe and rolling circle amplification (RCA) to detect FEN1. Our group members have utilized fluorescence assay to detect FEN1 in living cells. Biomineralized metal-organic framework nanoparticles (ZIF-8 NPs) were used to codeliver the encapsulated proteins and DNA probes to living cells for sensitive detection of FEN1 (Tang et al., 2021).

Nanoparticles as containers have shown great potential in tumor-targeted delivery, controlled drug release and improved drug bioavailability (Gao et al., 2020; Zhang et al., 2019, 2021). For example, Chu et al. developed biomineralized metal-organic framework nanoparticles (MOF NPs) as a carrier system for intracellular codelivery of enzymes and nucleic acid probes (Zhang et al., 2019). Tang et al. designed a drug delivery system in which AuNCs were employed as a drug carrier to perform specific cancer cell recognition, controlled drug release and effective comprehensive therapy (Tang et al., 2013). As a container, mesoporous silica nanoparticles (MSNs) have been applied in various fields of controlled release technology due to their high surface area, large pore volume, bio-compatibility and ease of surface functionality. The volume and release behavior of cargos can be better controlled by surface functionalization (Ma et al., 2020; Tan et al., 2019; Wang et al., 2020b; Zhu et al., 2021). Therefore, MSNs are a promising candidate carrier for loading a wide range of substances, such as drugs, and fluorescence molecules.

For mesoporous material, it is important to select a gatekeeper of suitable size and properties. Gold nanoparticles (AuNPs) was connected with base sequence by adsorption. Compared with thymine (dT), AuNPs had a higher affinity with adenine (dA). The binding strength of AuNPs to poly dA sequences was greater than that of Au–S bond (Chen et al., 2017; Lu et al., 2017; Yang et al., 2018; Yue et al., 2020). Our group members have utilized this technology and designed a nanoprobe (AuNPs-polydA20-polydT20) for label-free imaging of FEN1 in living cells (Wang et al., 2020a). Single-stranded DNA (ssDNA) possess several characteristics, such as easy labeling, high affinity and specificity. Thus, we prepared the AuNPs modified with ssDNA (AuNPs-ssDNA) as gatekeepers to construct the controlled release system. Meanwhile, the preparation of AuNPs-ssDNA was simple, rapid, specific and easy to obtain.

To take advantage of the ingenious characteristics of MSNs and make use of the FEN1 recognition function, we designed a nanoprobe which assembled MSNs loaded with rhodamine 6G (Rh6G) and AuNPs-ssDNA to quantitatively detect FEN1 activity. In this work, the aminoated mesoporous nanopaticles (NH_2-MSNs) were firstly loaded with fluorescence molecules Rh6G. To prepare the AuNPs-ssDNA, dT20 at the 5′-end of ssDNA was modified with carboxyl group in end and dA20 at the 3′-end of ssDNA was effectively absorbed on the surface of AuNPs. Then, based on the chemical reaction of carboxyl and amino group, the AuNPs-ssDNA as gatekeepers blocked the cargos of NH_2-MSNs. As a result, the mesoporous nanopaticle nanoprobe (NH_2-MSNs-Rh6G@AuNPs-ssDNA) was constructed. The nanoprobe could sensitively detect FEN1 by the controlled-release method. Without FEN1, the fluorescence signal was weak due to the encapsulation effect of AuNPs-ssDNA. Once FEN1 was added, the ssDNA was specifically cleaved. As a result, AuNPs left the surface of NH_2-MSNs, and Rh6G was released from NH_2-MSNs pores, which caused fluorescence signal recovery. Thus, FEN1 activity was detected by this sensitive controlled-release technique. The fluorescence signal showed a good linear relationship with the logarithm of FEN1 activity ranging from 0.05 to 1.75 U, and the detection limit was 0.03 U. Moreover, confocal imaging demonstrated that this proposed biosensor could distinguish tumor cells from normal cells. Therefore, this technique contributes to clinical diagnostic and therapeutic monitoring.

2. Experimental section

2.1. Preparation of AuNPs-ssDNA

AuNPs were prepared according to the previous literature (Nam et al., 2003; Nie et al., 2009; Qin et al., 2017; Zhang et al., 2020a). The synthesis process was introduced in detail in the Supporting Information, Materials and Methods. The AuNPs-ssDNA were prepared according to the previous literature (Wang et al., 2020a). First, 100 μL of AuNPs (~18 nM) and 2 μL of ssDNA (100 μM) was mixed and reacted for 3 min. Second, 2 μL of citric acid solution (500 mM, pH 3.0) was added to the solution with 5 s vortex oscillation and then stood for 3 min. Then 6 μL of HEPES buffer-1 (500 mM, pH 7.0) was added to adjust the solution to neutral conditions. In the end, the excess ssDNA was removed by centrifugation, and the precipitates (AuNPs-ssDNA) were redissolved with HEPES buffer-2 (5 mM, pH 7.0).

2.2. Fabrication of aminoated mesoporous silica nanoparticles loaded with fluorescent molecules Rh6G (NH_2-MSNs-Rh6G)

The MSNs were prepared according to the previous literature (Ma et al., 2020; Tan et al., 2019). Briefly, 0.5 g hexadecyl trimethyl ammonium bromide (CTAB) was dissolved in 240 mL of ultrapure water under stirring and heated at 80 °C. As the solution gradually clarified and became transparent, 1.5 mL of sodium hydroxide (NaOH) solution was added and kept for 20 min. Then 2.5 mL of oftetraethyl orthosilicate (TEOS) was added slowly to the reaction solution, and stirred for 2 h until white precipitate appeared. Following that, the white solid was filtered, and washed successively with methanol and water, and dried in the air. In order to remove excess CTAB, the dried white solid was put into the mixed solution of ethanol and hydrochloric acid (50:1, by volume) and refluxed for 10 h. After that, the reaction solution was centrifuged at 5000 rpm for 5 min and washed three times with methanol and water. The resulted solid was placed at 60 °C and dried in vacuum for 4 h to obtain MSNs.

Next, NH_2-MSNs were synthesized according to the previous report (Tang et al., 2014). In brief, 0.5 g MSNs was dispersed in ethanol solution. Then 1.5 mL of 3-aminopropyltriethoxysilane (APTES) was added and refluxed for 8 h. After reaction, the mixture was washed with ethanol and centrifuged to remove excess APTES. The NH_2-MSNs were obtained after washed with water several times.

To obtain the NH_2-MSNs-Rh6G, 30 mg NH_2-MSNs were dispersed in 500 μL of Rh6G solution (4 μM) and incubated for 12 h. The resulting suspension was centrifuged at 5000 rpm for 5 min and washed three times with 0.01 M phosphate buffer solution (1 × PBS; 137 mM NaCl, 10 mM NaH_2PO_4, 2.7 mM KCl, 2 mM KH_2PO_4, pH 7.4). The obtained precipitate was dissolved in 500 μL of 1 × PBS solution.

2.3. Detection of FEN1 activity in vitro

The nanoprobe system was prepared according to the following procedure. The prepared NH_2-MSNs-Rh6G and AuNPs-ssDNA were mixed at a molar ratio of 650:1 and the entire volume was remained at 100 μL. After 6 h of reaction, the obtained nanoprobe system was measured by fluorescence method. Then the different concentrations of FEN1 were added to reaction buffer and incubated for 2 h at 37 °C. The fluorescence was excited at 490 nm and measured at 550 nm.

2.4. Selectivity assay

In order to test the selectivity of this method, different biological enzymes were tested. Final concentration of bovine serum albumin (BSA), telomerase, alkaline phosphatase (ALP), glucose oxidase (GOX), horse radish peroxidase (HRP) and poly (ADP-ribose) polymerase-1 (PARP-1) was 10 μg mL^{-1}, 2000 cells·mL^{-1}, 0.2 U·mL^{-1}, 5 mg mL^{-1}, 8 μg mL^{-1} and 1 U·mL^{-1}, respectively. The fluorescence was excited at

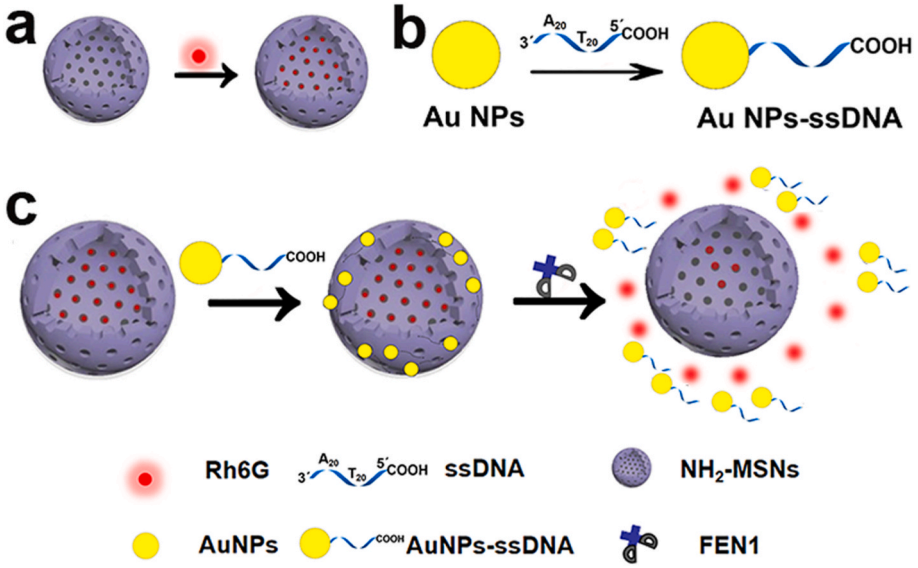

Scheme 1. Schematic illustration of the Rh6G-loaded MSNs@AuNPs-ssDNA nanoprobes for detection of FEN1. (a) Loading process of Rh6G into mesoporous silica nanoparticles; (b) synthesis process of the AuNPs-ssDNA; (c) assembly of NH_2-MSNs and AuNPs-ssDNA for analysis of FEN1 activity.

490 nm and measured at 550 nm.

2.5. Methyl thiazolyl tetrazolium (MTT) assay

In order to determine the toxicity and cell viability of the nanoprobes, MTT assay was performed. First, four kinds of cells were seeded at a density of 1×10^4 cells per well in 96-well plates for 24 h. Then, the medium was replaced by the medium containing nanoprobes, and incubated with the cells for 48 h, 32 h, 24 h, 18 h, 6 h and 2 h, respectively. After that, the cells in each well were treated with 200 μL of MTT solution (0.5 mg mL^{-1}, dissolved by 1 × PBS) for another 4 h at 37 °C. Finally, 150 μL of DMSO (AR) was added to each well and then shaken for 5 min. The cell viability data was obtained by using the microplate reader.

2.6. Confocal imaging of FEN1 in living cells

For imaging FEN1 in living cells with confocal fluorescence microscope, different kinds of cells were incubated in confocal dishes and seeded overnight. Next, a cell serum medium containing NH_2-MSNs-Rh6G@AuNPs-ssDNA was added for 6 h at 37 °C. Finally, to remove unnecessary nanoprobes, the confocal dishes were washed three times with 1 × PBS (pH 7.4).

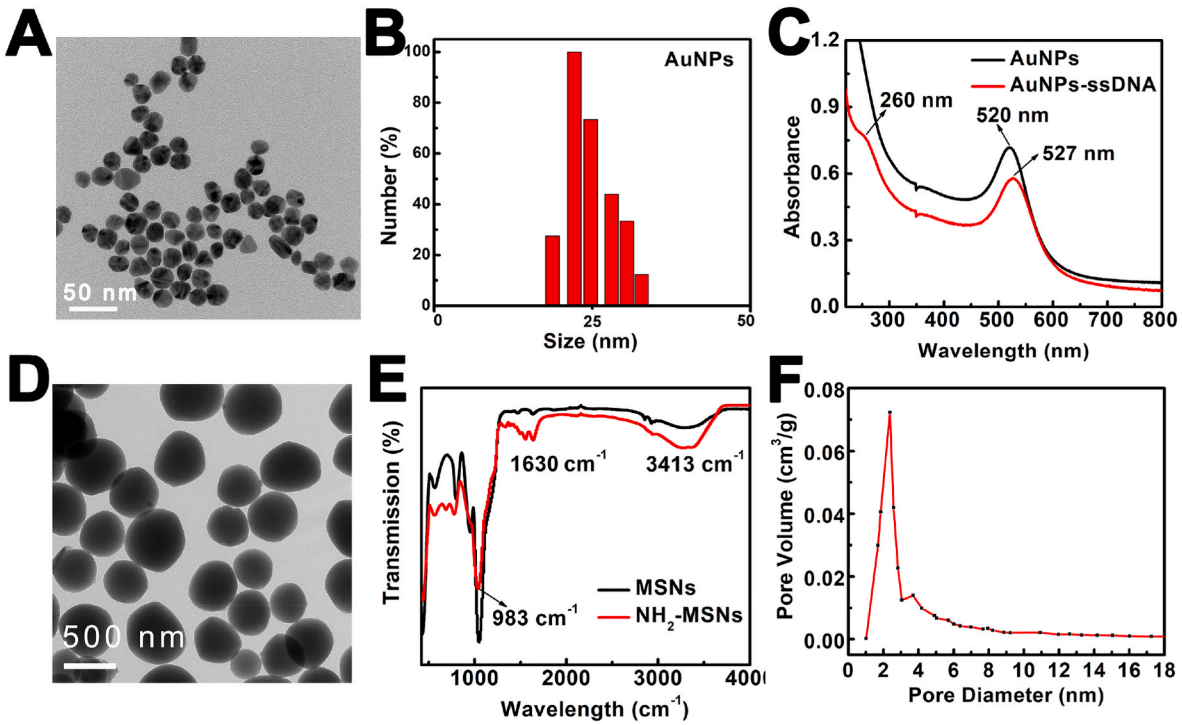

Fig. 1. (A) TEM image of AuNPs. (B) Size distribution of AuNPs. (C) UV–vis spectra of AuNPs and AuNPs-ssDNA. (D) TEM image of NH_2-MSNs. (E) FT-IR spectra of MSNs and NH_2-MSNs. (F) Pore diameter of NH_2-MSNs.

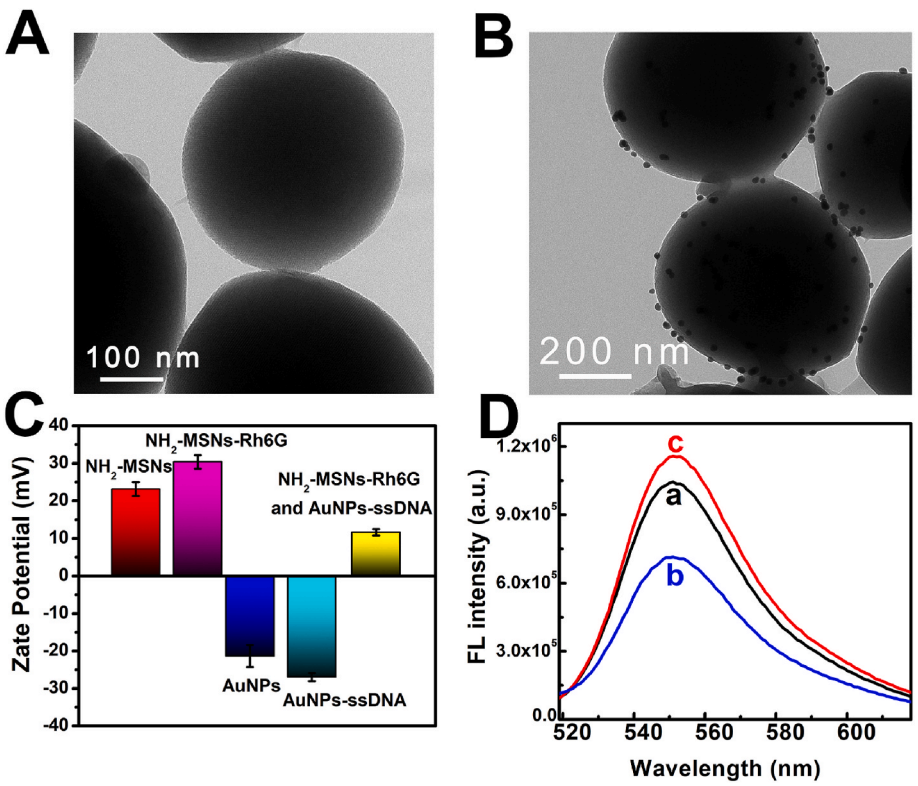

Fig. 2. (A) TEM image of NH_2-MSNs. (B) TEM image of NH_2-MSNs-Rh6G@AuNPs-ssDNA. (C) Zeta potentials of NH_2-MSNs, NH_2-MSNs-Rh6G, AuNPs, AuNPs-ssDNA and NH_2-MSNs-Rh6G@AuNPs-ssDNA. (D) Fluorescence responses of this assay. (a) NH_2-MSNs-Rh6G; (b) NH_2-MSNs-Rh6G@AuNPs-ssDNA; (c) NH_2-MSNs-Rh6G@AuNPs-ssDNA with FEN1.

3. Results and discussion

3.1. Principle for FEN1 detection

The detection principle of FEN1 was shown in Scheme 1. NH_2-MSNs were firstly loaded with fluorescence molecules Rh6G (Scheme 1a). For forming AuNPs-ssDNA, the carboxyl groups at the 5′ flaps of ssDNA overhanging, and poly dA20 at the 3′ flaps of ssDNA was effectively absorbed on the surface of AuNPs (Scheme 1b). Then AuNPs were assembled on the surface of MSNs due to the interaction between carboxyl and amino groups to further encapsulate Rh6G molecules. Under these circumstances, the fluorescence signal was weak. In the presence of FEN1, it recognized and cleaved the 5′ flaps of ssDNA. As a result, AuNPs leaved the surface of MSNs and the fluorescence molecules were released from MSNs pores. By this controlled-release method, different concentrations of FEN1 activity could be detected according to the recovery of fluorescence signals (Scheme 1c).

3.2. Synthesis of AuNPs-ssDNA

Various methods were used to prove that the AuNPs were modified with ssDNA. As shown in Fig. 1A, the spherical structure of the AuNPs was observed by a transmission electron microscope (TEM). In Fig. 1B, the dynamic light scattering (DLS) spectrogram had showed that the particle size of AuNPs was 18 nm, which was consistent with the TEM data. The sequence of single strands DNA (ssDNA) was shown in Table S1. As revealed in Fig. 1C, AuNPs had a UV–vis absorption peak at 520 nm. After modified with ssDNA, there was a small red shift of 6 nm, which indicated that AuNPs was successfully modified with ssDNA. Meanwhile, the peak located at 260 nm represented the specific absorption of DNA (Improta et al., 2016; Zhang et al., 2012). All these results demonstrated the successful formation of AuNPs-ssDNA.

3.3. Synthesis of NH_2-MSNs

Firstly, MSNs were obtained and then modified with amino groups. In order to prove that the synthesis of NH_2-MSNs was successful, the morphology of MSNs and NH_2-MSNs were observed by TEM. In Fig. S1, the TEM image showed the spherical structure of MSNs. The TEM image of NH_2-MSNs was shown in Fig. 1D. The surface functionalization of nanoparticles could be further characterized by fourier transform infrared spectroscopy (FT-IR). In Fig. 1E, the spectral image of NH_2-MSNs showed a strong broad band of 3413 cm^{-1}, which corresponds to $–NH_2$ stretching vibration, and broad peak at 983 cm^{-1} was attributed to the Si–O asymmetric stretching vibration. Compared with MSNs, the infrared spectrum of NH_2-MSNs showed that the absorption peak was located at 1630 cm^{-1}, which reflected the deformation vibration in the N–H bond in-plane. After MSNs modified with amino groups, the spectral vibration peaks could be observed at 1340 cm^{-1} and 1410 cm^{-1}, which belonged to the stretching bands of C–N group (Tao et al., 2014; Zhang et al., 2021). It shows that NH_2-MSNs have been successfully synthesized. The pore size of NH_2-MSNs was about 2.3 nm obtained by Brunauer-Emmett-Teller (BET) method (Fig. 1F). The typical isotherm of NH_2-MSNs was exhibited with nitrogen sorption technique (Fig. S2). These results all showed that NH_2-MSNs were synthesized successfully.

3.4. Synthesis of NH_2-MSNs-Rh6G@AuNPs-ssDNA

Due to the interaction between amino and carboxyl groups, AuNPs-ssDNA blocked the pores of NH_2-MSNs. Compared with the TEM image of NH_2-MSNs (Fig. 2A), it was obvious that NH_2-MSNs were sealed by the AuNPs-ssDNA (Fig. 2B). At the same time, prepared materials were characterized by zeta potential method. In Fig. 2C, as expected, the zeta potential of the NH_2-MSNs was +23.16 mV, and the zeta potential of NH_2-MSNs-Rh6G was +30.38 mV. In contrast, the unmodified AuNPs showed a negative zeta potential (−21.32 mV), and the zeta potential of

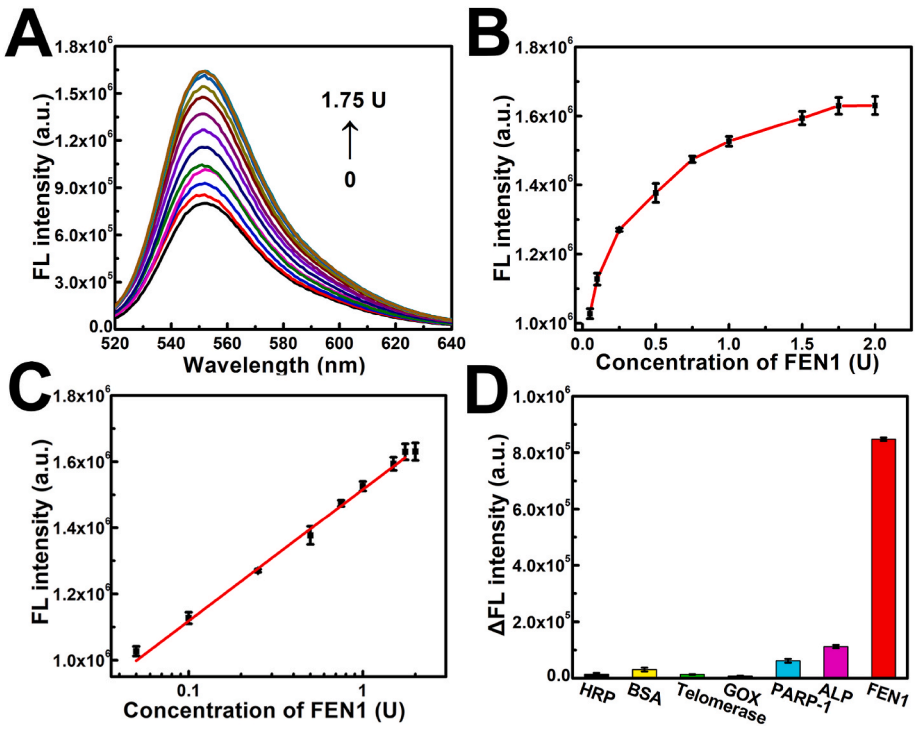

Fig. 3. (A) Fluorescence spectra of the mesoporous silica nanoparticles probe after reacting with FEN1. The concentration of FEN1 ranged from 0 to 1.75 U. (B) Plot of the fluorescence intensity as a function of FEN1 concentration ranging from 0.05 to 2.0 U. (C) The fluorescence intensity linear relationship with the concentration logarithmic (lg) value of FEN1. (D) Selectivity of the proposed nanoprobe.

AuNPs-ssDNA was −26.93 mV. After the AuNPs-ssDNA reacting with NH_2-MSNs-Rh6G, the zeta potential of NH_2-MSNs-Rh6G@AuNPs-ssDNA was +11.62 mV. These characterization results all proved that the AuNPs-ssDNA reacted with NH_2-MSNs and blocked the pores.

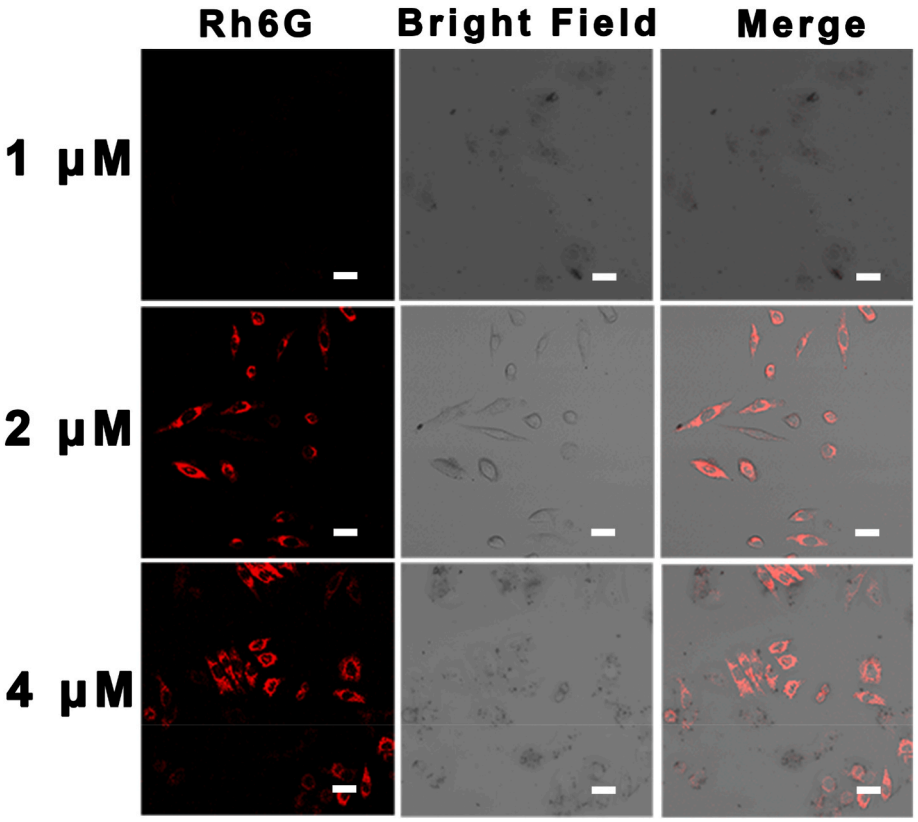

Fig. 4. Fluorescence confocal images of HepG2 cells incubated with different concentration of NH_2-MSNs-Rh6G@AuNPs-ssDNA nanoprobe (scale bar: 30 μm).

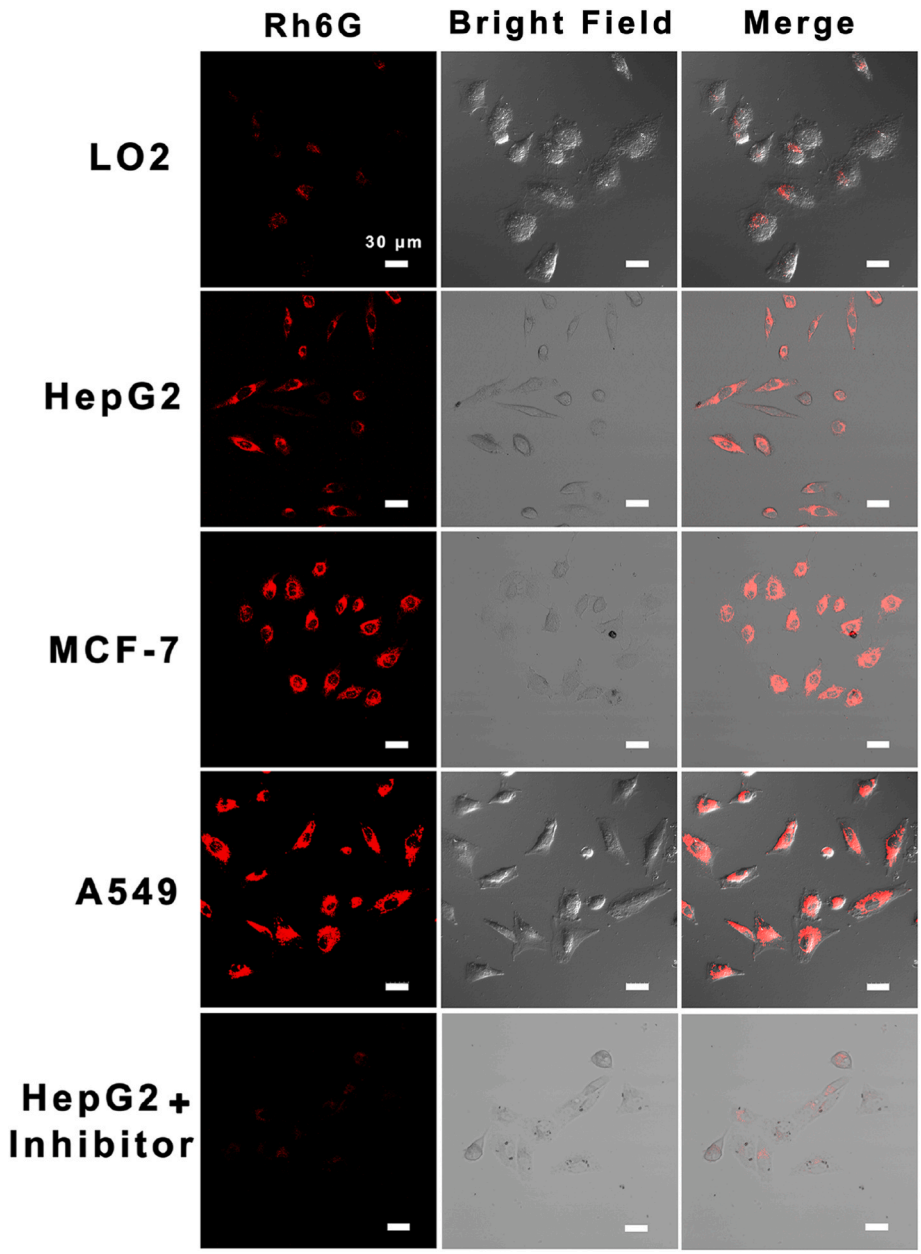

Fig. 5. Fluorescence confocal images of normal (LO2), tumor cells (MCF-7, A549, HepG2) after incubated with 2 μM NH_2-MSNs-Rh6G@AuNPs-ssDNA nanoprobe for 6 h. Bottom: Inhibition of ATA on HepG2.

3.5. Optimization of the experimental conditions

To determine the optimal conditions for FEN1 detection, some experiment parameters were optimized including the ratio of NH_2-MSNs-Rh6G and AuNPs-ssDNA, Rh6G solutions concentration, reaction time, and buffer solution. In Fig. S3A, when the molar ratio NH_2-MSNs-Rh6G and AuNPs-ssDNA was 650:1, the fluorescence signals reached the minimum, obtaining the maximum blocking effect. Therefore, the optimal molar ratio was 650:1. As shown in Fig. S3B, the relatively stable fluorescent signal appeared in 2 h, so the optimal reaction time was 2 h. The buffer solution in experiment was 0.01 M phosphate buffer (1 × PBS), and the solution optimal pH was 7.4 (Fig. S3C), which was also suitable for subsequent cell experiments. The optimal concentration of Rh6G was investigated (Fig. S3D). 4 μM of Rh6G was selected for in vitro experiment. The relationship between Rh6G release kinetic rate and fluorescence intensity was studied (Fig. S6).

3.6. Performance of detection of FEN1 activity in vitro

The fluorescence responses were used to illustrate the feasibility of this assay. As shown in Fig. 2D, the fluorescence intensity of the NH_2-MSNs-Rh6G was high (the black curve). After the AuNPs-ssDNA encapsulating Rh6G molecules, the fluorescence intensity decreased significantly (the blue curve), which demonstrated that AuNPs-ssDNA blocked the pores of NH_2-MSNs successfully. When FEN1 was added, it could identify and cleave the 5′ flaps of ssDNA. As a result, AuNPs leaved the surface of MSNs and the Rh6G were released from MSNs inner. Under these circumstances, the fluorescence signal recovered obviously (the red curve), revealing that the controlled-release strategy could be applied to detect FEN1.

Under the optimal conditions, as shown in Fig. 3A, fluorescence intensity at 550 nm was related to FEN1 at different concentrations. In Fig. 3B, it showed the linear curve relationship between FEN1 concentration and fluorescence intensity. As shown in Fig. 3C, the fluorescence

Table 1
Assay results for detection of FEN1 in human serum samples.

Added (U)	Found (U)	Recovery (%)	RSD (%, n = 3)
0.050	0.0499	99.79	3.36
0.1000	0.0949	94.86	1.22
0.5000	0.4942	98.84	2.20
1.0000	0.9574	95.47	2.82
1.5000	1.4375	95.63	3.83

intensity had a good linear relationship with the logarithm of FEN1 concentration. The corresponding FEN1 concentration range was from 0.05 to 1.75 U, and the detection limit was calculated to be 0.03 U. The linear equation was calibrated as FL = 1516000.00 + 397586.17 lg C_{FEN1} (R^2 = 0.993). These results demonstrated that the proposed fluorescence analysis for FEN1 had a wide linear range and high sensitivity, which has been compared with previous reported methods in Table S3.

To assess the nanoprobes selectivity for detection of FEN1, other interference targets such as HRP, BSA, telomerase, GOX, PARP-1, and ALP were investigated. In Fig. 3D, it showed that these control substrates had no obvious fluorescence recovery, indicating that there was no enzymatic digestion reaction. Thus, the proposed nanoprobe had high specificity for FEN1 detection, and the sensitivity of this method was verified.

3.7. Imaging of FEN1 in living cells

MTT assay was carried out to evaluate the toxicity of the nanoprobes in different cells. In Fig. S4, it showed that all cells still maintained a survival rate of at least 80% after incubated with the proposed nanoprobes, which indicated that the proposed nanoprobes had low toxicity and good biocompatibility.

Then, FEN1 imaging in living cells was performed under a laser scanning confocal microscope (LSCM). First, the HepG2 cells were selected as models to optimize the concentration of nanoprobes entering the cells. As shown in Fig. 4, there was almost no fluorescence in cells treated with 1 μM nanoprobes, indicating that few nanoprobes entered into cells. When the concentration of nanoprobes was 2 μM or 4 μM, the cell images all showed significant fluorescence, and the fluorescence intensity was similar. Therefore, we chose 2 μM nanoprobes for subsequent cell experiments.

Then, under the optimal concentration of nanoprobe, cell experiments were performed using LO2, MCF-7, A549, and HepG2 cells. As displayed in Fig. 5, the cancer cells (MCF-7, A549, and HepG2) had strong fluorescence compared with normal cells (LO2). To prove that the change of fluorescent signal was induced by FEN1 activity, 2 μM of aurintricarboxylic acid (ATA) was used to down regulate FEN1 expression in HepG2 cell. The CLSM image in Fig. 5 showed that ATA pretreated HepG2 cells showed a greatly decreased fluorescence signal, indicating that the signal intensity was associated with FEN1 activity. According to the cell laser confocal diagram in Fig. 5, the change of fluorescence intensity was processed to obtain a column figure (Fig. S5). The results revealed that the content of FEN1 in tumor cells is obviously higher than that in normal cells, and this strategy could be used to distinguish cancer cells from normal cells.

3.8. Performance of the proposed nanoprobe

To determine the analytical performance in complex biological matrix, the proposed nanoprobe was applied in human serum to analyze FEN1. As shown in Table 1, experimental results showed that the recoveries of different concentrations of FEN1 varied from 94.86% to 99.79%, and the relative standard deviations were from 1.22% to 3.83%.

The nanoprobe was applied to the cytoplasm and nucleus of four kinds of cells. In Table S2, the results indicated that FEN1 exists in both tumor normal cells and human cells, but the content of FEN1 in tumor cells (A549, HepG2, and MCF-7) is obviously higher than that in normal cells (LO2). These results were consistent with previous reports (Guo et al., 2008; Wang et al., 2014), which demonstrated that the nanoprobe has a good application prospect in practical samples.

4. Conclusions

In this work, we successfully designed a controlled-release nanoprobe for detection of FEN1 activity. The detection method for FEN1 was simple, reliable, accurate, and selective. The fluorescence signal of nanoprobe gradually increased with the increase of FEN1 concentration. The proposed method was successfully applied to detect FEN1 activity sensitively. The linear detection range of FEN1 was from 0.05 to 1.75 U, and the detection limit was 0.03 U. Besides, the established strategy was applied to image FEN1 in living cells for distinguishing cancer cells from normal cells, which holds great potential for clinical diagnosis and FEN1-based drug development.

CRediT authorship contribution statement

Yanhua Tang: Methodology, Data curation, Writing – original draft. **Duoduo Zhang:** Conceptualization, Methodology, Writing – review & editing. **Ye Lu:** Methodology. **Songqin Liu:** Supervision. **Juan Zhang:** Writing – review & editing. **Yuepu Pu:** Supervision. **Wei Wei:** Supervision, Project administration, Writing – review & editing.

Declaration of competing interest

The authors declare that they have no known competing financial interests or personal relationships that could have appeared to influence the work reported in this paper.

Acknowledgments

This work was supported by research grants from National Natural Science Foundation of China (81730087, 81872645, and 81573189).

Appendix A. Supplementary data

Supplementary data to this article can be found online at https://doi.org/10.1016/j.bios.2022.114529.

References

Balakrishnan, L., Bambara, R.A., 2013. Annu. Rev. Biochem. 82, 119–138.
Chen, L.Z., Chao, J., Qu, X.M., Zhang, H.B., Zhu, D., Su, S., Aldalbahi, A., Wang, L.H., Pei, H., 2017. ACS Appl. Mater. Interfaces 9, 8014–8020.
Guo, E., Ishii, Y., Mueller, J., Srivatsan, A., Gahman, T., Putnam, C.D., Wang, J.Y.J., Kolodner, R.D., 2020. Proc. Natl. Acad. Sci. U.S.A. 117 (32), 19415–19424.
Guo, Z.G., Qian, L.M., Liu, R., Dai, H.F., Zhou, M., Zheng, L., Shen, B.H., 2008. Mol. Cell. Biol. 28, 4310–4319.
Gao, W.X., Liu, Y., Zhang, H.R., Wang, Z.H., 2020. ACS Sens 5, 1216–1222.
He, L.F., Zhang, Y.L., Sun, H.F., Jiang, F., Yang, H., Wu, H., Zhou, T., Hu, S.C., Kathera, C. S., Wang, X.J., Chen, H.Y., Li, H.Z., Shen, B.H., Zhu, Y.Q., Guo, Z.G., 2016. EBioMedicine 14, 32–43.
Improta, R., Santoro, F., Blancafort, L., 2016. Chem. Rev. 116 (6), 3540–3593.
Kao, H.I., Henricksen, L.A., Liu, Y., Bambara, R.A., 2002. J. Biol. Chem. 277, 14379–14389.
Lam, J., Seligson, D., Yu, H., Li, A., Eeva, M., Pantuck, A., Zeng, G., Horvath, S., 2006. A. S. BJU Int. 98, 445–451.
Li, B.Z., Xia, A.Q., Xie, S.Y., Lin, L., Ji, Z.R., Suo, T., Zhang, X., Huang, H., 2021. Anal. Chem. 93 (6), 3287–3294.
Lu, C., Huang, Z.C., Liu, B.W., Liu, Y.B., Ying, Y.B., Liu, J.W., 2017. Angew. Chem. Int. Ed. 56, 6208–6212.
Lu, X., Liu, R., Wang, M.N., Kumar, A.K., Pan, F.Y., He, L.F., Hu, Z.G., Guo, Z.G., 2020. Oncogene 39, 234–247.
Ma, L., Cao, X.Q., Wang, H.Y., Lu, K., Wang, Y., Tu, C.H., Dai, Y.J., Meng, Y.Y., Li, Y.Y., Yu, P., Man, S.L., Diao, A.P., 2019. J. Agric. Food Chem. 67, 1656–1665.
Ma, N., Ren, X., Wang, H., Kuang, X., Fan, D., Wu, D., Wei, Q., 2020. Anal. Chem. 92, 14069–14075.

Nam, J., Thaxton, C., Mirkin, C., 2003. Sci 301, 1884–1886.
Nie, H., Liu, S., Yu, R., Jiang, J., 2009. Angew. Chem., Int. Ed. 48, 9862–9866.
Nikolova, T., Christmann, M., Kaina, B., 2009. Anticancer Res 29, 2453–2459.
Pike, J.E., Henry, R.A., Burgers, P.M.J., Campbell, J.L., Bambara, R.A., 2010. J. Biol. Chem. 285, 41712–41723.
Qin, L., Zeng, G.M., Lai, C., Huang, D.L., Zhang, C., Xu, P., Hu, T.J., Liu, X.G., Cheng, M., Liu, Y., Hu, L., Zhou, Y.Y., 2017. Sens. Actuators B. 243, 946–954.
Tang, D.P., Lin, Y.X., Zhou, Q., Lin, Y.P., Li, P.W., Niessner, R., Knopp, D., 2014. Anal. Chem. 86, 11451–11458.
Tang, D.P., Liu, B.Q., Niessner, R., Li, P.W., Knopp, D., 2013. Anal. Chem. 85, 10589–10596.
Tan, H.X., Ma, L., Guo, T., Zhou, H.Y., Chen, L., Zhang, Y.H., Dai, H.J., Yu, Y., 2019. Anal. Chim. Acta 1068, 87–95.
Tang, Y.F., Wei, W., Liu, Y., Liu, S.Q., 2021. Anal. Chem. 93, 4960–4966.
Tao, C.L., Zhu, Y.F., Xu, Y., Zhu, M., Moritac, H., Hanagata, N., 2014. Dalton Trans 43, 5142.
Thompson, M., Gotham, V., Ciani, B., Grasby, J.A., 2018. Nucleic Acids Res 46, 7858–7872.
Wang, C.C., Zhang, D.D., Tang, Y.F., Wei, W., Liu, Y., Liu, S.Q., 2020a. ACS Appl. Bio Mater. 3, 4573–4580.
Wang, J., Li, B.X., Pu, X.M., Wang, X.M., Cooper, R.C., Gui, Q., Yang, H., 2020b. ACS Appl. Mater. Interfaces 12, 10202–10210.
Wang, K.J., Xie, C.H., Chen, D.R., 2014. Int. J. Mol. Med. 33, 1268–1274.
Yang, K., Wang, H.Z., Ma, N., Zeng, M., Luo, H.Q., He, D.G., 2018. ACS Appl. Mater. Interfaces 10, 44546–44553.
Yue, Q., Sun, J.G., Kang, Y.J., Deng, Y.H., 2020. Angew. Chem. Int. Ed. 59, 15804–15817.
Zhang, B., Liu, B.Q., Tang, D.P., Niessner, R., Chen, G.N., Knopp, D., 2012. Anal. Chem. 84 (12), 5392–5399.
Zhang, D.D., Wang, K., Wei, W., Liu, S.Q., 2020a. ACS Sens 5 (4), 1198–1206. https://doi.org/10.1021/acssensors.0c00264.
Zhang, H., Ba, S., Mahajan, D., Lee, J.Y., Ye, R.J., Shao, F.W., Lu, L., Li, T.H., 2018a. Nano Lett 18, 7383–7388.
Zhang, H., Gao, Z., Li, X.X., Lu, L., Ye, S.J., Tang, B., 2021a. Chem. Sci 12, 12429–12436.
Zhang, J., He, M.Y., Nie, C.P., He, M.M., Pan, Q.S., Liu, C., Hu, Y.L., Yi, J.T., Chen, T.T., Chu, X., 2019. Anal. Chem. 91, 9049–9057.
Zhang, K.Q., Keymeulen, S., Nelson, R., Tong, T.R., Yuan, Y., Yun, X.W., Liu, Z., Lopez, J., Raz, D., Kim, J., 2018b. Am. J. Pathol. 188, 242–251.
Zhang, Y.Y., Liu, X., Liu, L.W., Chen, J.N., Hu, Q.Y., Shen, S., Zhou, Y.J., Chen, S.Y., Xue, C., Cui, G.Y., Yu, Z.J., 2020b. Dis. Markers 17, 2514090.
Zhang, Y., Xiong, M.T., Ni, X.M., Wang, J.R., Rong, H.H., Su, Y.Q., Yu, S.H., Mohammad, I.S., Leung, S.S.Y., Hu, H.Y., 2021b. ACS Appl. Mater. Interfaces 13 (15), 18077–18088.
Zheng, L., Jia, J., Finger, L.D., Guo, Z.G., Zer, C., Shen, B.H., 2011. Nucleic Acids Res 39, 781–794.
Zhou, B., Lin, L., Li, B.Z., 2021. Sens. Actuators B. 346 https://doi.org/10.1016/j.snb.2021.130457.
Zhu, A.F., Jiao, T.H., Ali, S.J., Xu, Y., Qin, O., Chen, Q.S., 2021. Anal. Chem. 93, 9788–9796.